LAWRENCE
LIVERMORE
NATIONAL
LABORATORY

LLNL-JRNL-663803

Modeling and Uncertainty Quantification of Vapor Sorption and Diffusion in Heterogeneous Membranes and Materials

Y. Sun, S. J. Harley, E. A. Glascoe

November 5, 2014

ChemPhysChem

Disclaimer

Modeling and Uncertainty Quantification of Vapor Sorption and Diffusion in Heterogeneous Membranes and Materials

Yunwei Sun, Stephen J. Harley, Elizabeth A. Glascoe[1]

Lawrence Livermore National Laboratory, 7000 East Avenue, Livermore, California 94550, USA

Received: 10 November 2014; Accepted: ;/Published online:

Abstract

A high-fidelity model of kinetic and equilibrium sorption and diffusion is derived and exercised. The gas-diffusion model is coupled with a triple-sorption mechanism: Henry's law absorption, Langmuir adsorption, and pooling or clustering of molecules at the higher partial pressures. Sorption experiments were conducted previously and span a range of relative humidities (0∼95%) and temperatures (30∼60 °C). Reaction rates of sorption processes and effective diffusivity are determined by minimizing the absolute difference between measured and modeled uptakes. Uncertainty quantification and sensitivity analysis methods are described and exercised here to demonstrate the capability of this modeling approach. Water uptake in silica filled- and unfilled-poly(dimethylsiloxane) (PDMS) networks was investigated here, however, the model is versatile enough to be used with a wide range of materials and vapors.

Keywords: Vapor, Sorption, Diffusion, Henry's Law, Langmuir, Pooling, Membrane.

[1]Corresponding author. Tel.: (925) 424-5194; fax (925) 424-3281; E-mail adress: glascoe2@llnl.gov (E.A. Glascoe).

Nomenclature

Symbol	Unit	Definition	Where
α	[-]	Lumped pooling coefficient	Eq. (6)
A_0	[cm^2]	Sample area	Eq. (12)
b'	[g mg^{-1}]	Langmuir affinity constant $k_{\text{ads}}/k_{\text{des}}$	Eq. (5)
c	[mg cm^{-3}]	Vapor concentration in gas phase per unit pore volume	Eq. (2)
C	[mg g^{-1}]	Total vapor concentration per unit of material mass	Eq. (1)
C_{H}	[mg g^{-1}]	Vapor concentration in Henry's mode per unit of material mass	Eq. (3)
C'_{H}	[mg g^{-1}]	Langmuir capacity constant per unit material mass	Eq. (4)
C^0_{H}	[mg g^{-1}]	Threshold of Henry's concentration at which pooling occurs	Eq. (10)
C_{L}	[mg g^{-1}]	Vapor concentration in Langmuir mode per unit material mass	Eq. (4)
C_{P}	[mg g^{-1}]	Vapor concentration in pooling mode per unit material mass	Eq. (6)
D	[cm^2 min^{-1}]	Diffusion coefficient	Eq. (1)
D_0	[cm^2 min^{-1}]	Diffusivity	Eq. (1)
f	[mg min]	Objective function for system calibration	Eq. (11)
$\mathcal{H}$	[-]	Heaviside step function	Eq. (10)
K'_{C}	[-]	Equilibrium constant for clustering reaction	Eq. (6)
k_{ads}	[g min^{-1}mg^{-1}]	Adsorption rate	Eq. (3)
k_{des}	[min^{-1}]	Desorption rate	Eq. (3)
k_{d}	[cm^3 g^{-1}]	Henry's law constant	Eq. (6)
λ	[mg g^{-1}]	Mass uptake per gram of bulk and dry PDMS	Eq. (13)
λ_i	[mg g^{-1}]	Partial mass uptake per gram of bulk and dry PDMS	Eq. (14)
m	[mg]	Modeled moisture uptake	Eq. (11)
$\hat{m}$	[mg]	Measured moisture uptake	Eq. (11)
n	[-]	Pooling-power constant	Eq. (6)
ϕ	[cm^3 cm^{-3}]	Porosity, void volume per unit bulk volume	Table 1
ϕ_e	[cm^3 cm^{-3}]	Effective porosity contributing to transport	Table 2
ρ_{b}	[g cm^{-3}]	Sample bulk density	Eq. (12)
RH	[-]	Relative humidity %	Table 4
S	[mg g^{-1}]	Vapor concentration of empty Langmuir sites	Eq. (3)
T	[°C]	Temperature	Table 1
t	[min]	Time	Eq. (1)
t_λ	[min]	Time required to reach equilibrium	Table 4
τ	[-]	Tortuosity of PDMS	Eq. (1)
x	[cm]	Distance	Eq. (1)
x_l	[cm]	PDMS thickness	Eq. (13)

1. Introduction

The sorption of vapors and gases into a material is important to consider when assessing the transport and permeability of a membrane, especially in non-equilibrium conditions. Sorption can retard transport, alter the nature of the material via plasticization, and result in outgassing of the vapor at a later time if the surrounding conditions change.

Accurately and precisely characterizing the sorption and diffusion properties of a vapor in a membrane or material, especially a heterogeneous material, is challenging. The two processes are material and vapor dependent and occur concomitantly in non-equilibrium conditions. The reward for a well-developed and validated model is the ability to characterize a variety of materials and predict material response under a range of conditions.

Recent improvements in the technology for experimentally measuring vapor uptake or outgassing have made it easy to collect high-fidelity data. One can extract a great deal of information about how a vapor diffuses through and interacts with the material using relatively simple models [1,2]. Currently, many researchers rely on established mathematical models to analyze and interpret their data [3,4]. These models are easy to use but lack the

sophistication and rigor to capture much of the physics that is implicit in the mechanisms of diffusion and sorption.

In this study, we developed a continuum-scale model and a computer code for describing the vapor diffusion in a heterogeneous material (e.g., a silica filled polymer). Our model is an improvement over published approaches [5,6,7] and is developed on a triple-mode sorption mechanisms [8,9], in which Henry's law absorption, Langmuir adsorption, and pooling sorption are coupled. Gas transport in poly(dimethylsiloxane) (PDMS) materials has been extensively studied using sorption-diffusion models (e.g., [8, 10-16]). The accurate simulation of gas sorption and diffusion at the microscale has been a challenge in industrial and academic communities due to the complicated pore structure of materials. The most rigorous approach for dealing with these materials involves solving mass-balance equations at the micro or sub-microscopic scale; which is computationally expensive and requires detailed calculations of the material dynamics (e.g., polymer chain motions etc.). Our treatment using continuum-scale models with effective diffusion and sorption is significantly more efficient and practical for comparing and interpreting experimental data. Penetrant or vapor-species diffusivity is treated as an *effective diffusivity* (or diffusion coefficient) that captures both the interactions of the vapor with the material (e.g., van der Waals interactions) and the material-specific tortuosity.

We have integrated our sorption-diffusion model with an existing code, PSUADE [17] to calibrate system parameters and to conduct global sensitivity analysis and uncertainty quantification. To the best of our knowledge, no study has included dynamic pooling mechanisms in the model or expanded the codes to perform uncertainty quantification (UQ). With this model, we can rigorously characterize and quantify the sorption and diffusion of vapor in heterogeneous materials directly from experimental data and predict these processes for realistic scenarios.

The materials studied here are PDMS polymers, which represent porous and heterogeneous media. PDMS has been widely used as moisture barriers in industry because it is nontoxic and relatively hydrophobic [8,16,18-19]. Fillers, such as silica, are frequently added to increase mechanical and tear strength, however, these fillers are significantly more hydrophilic than the PDMS-matrix resulting in a heterogeneous material [9,20-21]. Our experiments focus on moisture sorption and diffusion in two different materials: (1) an unfilled- and (2) a filled-PDMS network, however, the models developed here are applicable to other heterogeneous materials and other penetrant molecules besides water.

2. Methods

2.1. Experimental Data

Experiments measuring the dynamic vapor sorption isotherms in (1) an ideal- (unfilled-) and (2) a filled-PDMS network were conducted using the IGAsorp Instrument developed by Hiden Isochema. The experiments and instrument are described in detail previously [8,9]. Briefly, the filled PDMS network contained approximately 25% (wt) silica filler and the ideal-PDMS network was a synthesized material free of filler. The isotherms were acquired in steps of 5% relative humidity (RH) between 0 and 95% RH at 4 different temperatures (30, 40, 50 and 60 °C) in the ideal PDMS and at 40 °C in the filled PDMS. The sample mass was monitored continuously and the sample was considered to be in equilibrium with the boundary vapor pressure (i.e., the RH in the sample chamber) when the sorption process was 97% complete and the mass change approached an asymptote.

Five sets of experimental data are used in this work for studying sorption and diffusion processes in two PDMS materials (ideal and filled). The sample geometry, properties, and experiment setup are given in Table 1.

Table 1. Sample properties and experiment setup. Density was estimated using caliper measurements at room temperature.

Exp.	Sample	Sample geometry [cm]			ρ_b	Time	RH	T
		Length	Width	Height	[g cm^{-3}]	[min]	[%]	[°C]
1	Ideal PDMS	2.540	1.270	0.202	0.9541	234.95	0∼90.37	30
2	Ideal PDMS	2.540	1.270	0.202	0.9541	221.46	0∼90.46	40
3	Ideal PDMS	2.540	1.270	0.202	0.9541	214.09	0∼90.19	50
4	Ideal PDMS	2.540	1.270	0.202	0.9541	216.10	0∼90.08	60
5	Filled PDMS	2.540	1.270	0.200	1.201	1976.30	0∼95.67	40

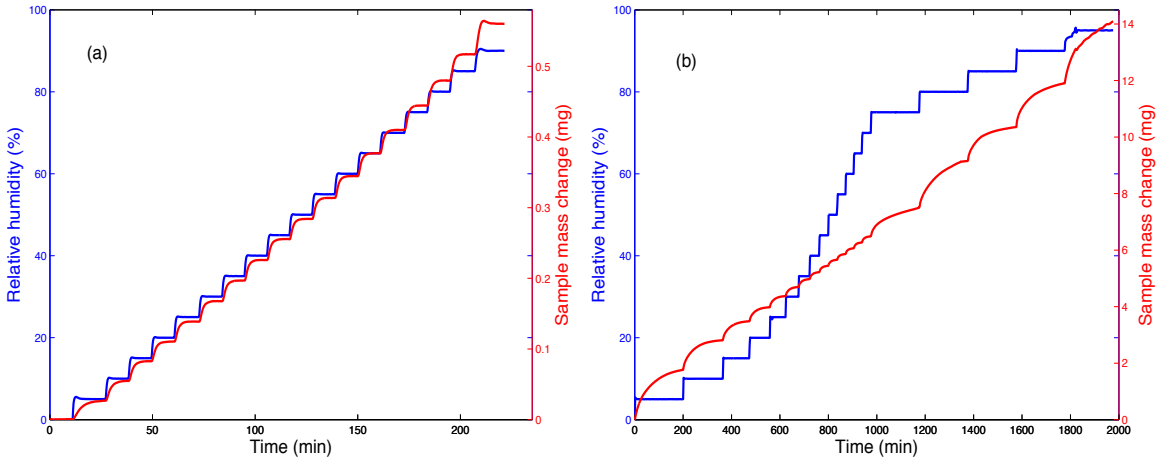

Figure 1. Relative humidity and corresponding mass change in Exp. 2 and Exp. 5 (Table 1) for (a) ideal and (b) filled PDMS at 40 °C.

Fig. 1 shows the relative humidity and sample mass response for both the ideal and filled PDMS at 40 °C; one can see clear differences in the mass response of the two materials. Most importantly, the filled PDMS sorbs over twenty times more water than that the ideal PDMS and takes significantly longer to reach equilibrium at each RH step. In addition, the filled PDMS sorbs the most water in the first two RH steps (RH<10%) and high RH steps (RH≥75%) whereas the ideal PDMS sorbs nearly the same amount in each RH step.

Fig. 2 is a plot of sample mass versus RH for each material and provides qualitative information about the mechanisms of sorption. The linear shape for the ideal-PDMS at four temperatures (30, 40, 50, and 60 °C in Fig. 2a) suggests that the dominant mechanisms in this material are diffusion and absorption (i.e., Henry's law absorption). The non-linear relationship in Fig. 2b indicates that moisture sorption is dominated by Langmuir and/or pooling mechanisms. In order to quantitatively characterize the mechanisms of sorption, we have developed a triple-mode sorption model coupled with a diffusion model. The model, which is described in Sect. 2.2, includes Henry's law absorption, Langmuir adsorption, and pooling mechanisms. An optimization model for mechanism calibration was developed and is described in Sect. 2.3.

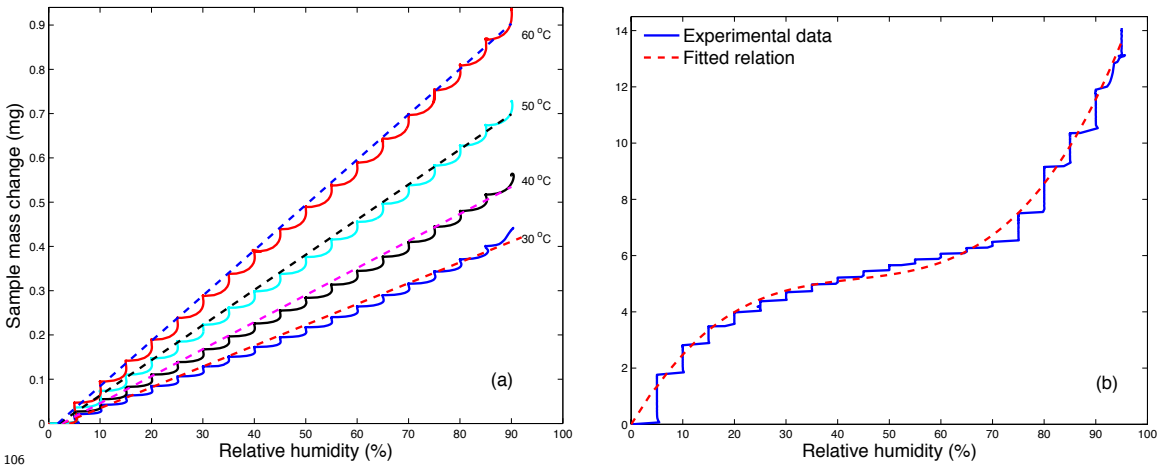

Figure 2. Relation between relative humidity and corresponding mass change for (a) ideal PDMS at 30, 40, 50, and 60 °C and (b) filled-PDMS at 40 °C. Dashed lines are fitted using MATLAB polyfit [22].

2.2. Sorption-Diffusion Model

The fundamental equation of gas diffusion coupled with kinetic Langmuir adsorption and equilibrium pooling sorption in a material is written

$$\frac{\partial C}{\partial t} = \frac{\partial \left(C_{\mathrm{H}} + C_{\mathrm{L}} + C_{\mathrm{P}}\right)}{\partial t} = D\frac{\partial^2 C_{\mathrm{H}}}{\partial x^2} \tag{1}$$

where C [mg g^{-1}] is the total concentration in terms of sample bulk mass, C_{H} [mg g^{-1}] is the mass concentration of the absorbed (i.e., Henry's mode) gas component (e.g., water vapor) per unit of sample bulk mass, C_{L} and C_{P} [mg g^{-1}] are the concentrations in Langmuir and pooling modes, respectively, and measured in mass of gas component per unit bulk mass of a material, D [cm^2 min^{-1}] is effective diffusion coefficient, t [s] is the time, and x [cm] is the distance. The effective diffusion coefficient is the product of molecular-weight dependent diffusivity and medium-specific tortuosity, $D = D_0\,\tau$, where D_0 [cm^2 min^{-1}] is diffusivity and τ [-] is a measure for the connectivity of pores and defined as the chord-arc ratio, which is the ratio of the straight distance to the integrated length of the tortuous pathway.

Our approach involves a single-phase sorption and diffusion rather than multi-phase (e.g., liquid and gas-phase) transport. To avoid modeling multiphase transport, Harley et al. (2012) [8] directly used Henry's concentration as a mobile species according to Henry's law sorption model

$$C_{\mathrm{H}} = k_{\mathrm{d}}\; c, \tag{2}$$

in which, c [mg cm^{-3}] symbolically represents gas-phase concentration of vapor and C_{H} is the concentration of water molecules that are mobile within the material (i.e., absorbed). Consequently, the Henry's law constant, k_{d}, is no longer required as a fitting parameter and is left as a fixed parameter in our modeling approach.

The kinetic adsorption and desorption is expressed as a reversible reaction [8]

$$S + C_{\mathrm{H}} \underset{k_{\mathrm{des}}}{\overset{k_{\mathrm{ads}}}{\rightleftharpoons}} C_{\mathrm{L}} \tag{3}$$

where k_{ads} [min^{-1}mg^{-1}g] and k_{des} [min^{-1}] are adsorption and desorption rates and S [mg g^{-1}] is the concentration of empty Langmuir sites. Then, the Langmuir concentration is expressed as

$$C_{\mathrm{L}} = C'_{\mathrm{H}} - S \tag{4}$$

where C'_{H} [mg g^{-1}] is the Langmuir capacity constant (reflecting available reactive surface sites).

Kinetic Langmuir sorption is expressed by differentiating (4)

$$\frac{\partial C_{\mathrm{L}}}{\partial t} = -\frac{\partial S}{\partial t} = k_{\mathrm{des}}\, b'\, S\, C_{\mathrm{H}} - k_{\mathrm{des}}\, (C'_{\mathrm{H}} - S)\,. \tag{5}$$

In Eq. (5), $b' = k_{\mathrm{ads}}/k_{\mathrm{des}}$ [mg^{-1}g] is Langmuir affinity constant. Equilibrium pooling sorption is expressed as a nonlinear function of local concentration in Henry's mode

$$C_{\mathrm{P}} = \frac{K'_{\mathrm{C}}(k_{\mathrm{d}} C_{\mathrm{H}})^n}{n} = \alpha\, C_{\mathrm{H}}^n, \quad \alpha = \frac{K'_{\mathrm{C}}\, k_{\mathrm{d}}^n}{n} \tag{6}$$

where K'_{C} [-] is equilibrium constant for clustering reaction, k_{d} [g^{-1} cm^3] is Henry's law constant, n represents the number of molecules in each pool and is treated as a fitting parameter at continuum scale. The dimension of K'_{C} is dependent on n. The mass change due to pooling sorption is

$$\frac{\partial C_{\mathrm{P}}}{\partial t} = \alpha\, n\, C_{\mathrm{H}}^{n-1} \frac{\partial C_{\mathrm{H}}}{\partial t}. \tag{7}$$

Substituting Eqs. (5) and (7) in Eq. (1), the system equations are written as

$$\left(1 + \alpha\, n\, C_{\mathrm{H}}^{n-1}\right) \frac{\partial C_{\mathrm{H}}}{\partial t} = D \frac{\partial^2 C_{\mathrm{H}}}{\partial x^2} - k_{\mathrm{des}}\, b'\, C_{\mathrm{H}}\, S + k_{\mathrm{des}}\, (C'_{\mathrm{H}} - S) \tag{8}$$

$$\frac{\partial S}{\partial t} = -k_{\mathrm{des}}\, b'\, S\, C_{\mathrm{H}} + k_{\mathrm{des}}\, (C'_{\mathrm{H}} - S)\,. \tag{9}$$

The pooling concentration is further modified as

$$C_{\mathrm{P}} = \alpha\, \mathcal{H}\left(C_{\mathrm{H}},\, C_{\mathrm{H}}^0\right) \left(C_{\mathrm{H}} - C_{\mathrm{H}}^0\right)^n \tag{10}$$

where C_{H}^0 is the threshold of Henry's concentration value, at which pooling sorption occurs, $\mathcal{H}$ is Heaviside step function (which equals to 1 $\forall C_{\mathrm{H}} > C_{\mathrm{H}}^0$ and 0 otherwise).

Equations (8) and (9) are solved by using an operator-splitting method. The diffusion operator is discretized using central finite difference accordingly to the sample thickness. Then, the algebraic equations are solved using LU factorization with backward substitution. Without considering advection, the coefficient matrix is symmetric and positive definite, we can use LU factorization without pivoting. The reaction operator, which is designed for modeling spatially independent processes, is solved by using MATLAB ode15s [22].

The mathematical model of vapor diffusion coupled with triple-mode sorption mechanism is developed as a deterministic simulator to describe water distribution in materials. The corresponding computer code is developed and implemented in MATLAB environment [22]. As the deterministic simulation provides the physical behavior of sorption and diffusion processes, the emulation (or response surface) from a certain number of simulations approximates the statistic relation between the output of interest and uncertain parameters, as well as uncertain formulation of physical processes. Then, the emulated model (e.g., in polynomial format) is used in the place of computationally expensive and high-fidelity simulator to evaluate objective functions and constraints for system calibration.

2.3. Surrogate Models for Optimization and Sensitivity Analyses

Parameter calibration and sensitivity analysis were accomplished, respectively, using Shuffled Complex Evolution (SCE) method [27] and sampling-based approach [26]. In the sampling-based, or non-intrusive, approach the Latin-Hypercube method [23] is used to generate many sample points (i.e., thousands) that sufficiently cover the parametric space. Each sample point consists of values for D, K_{des}, C'_{H}, b', α, C^o_{H}, n, and ϕ_e (see Table 3). Note that in the diffusion-only model in the ideal PDMS when relative humidity is low (RH <

40%), each sample point consisted of values for D and ϕ_e only. Each sample point is used to parameterize the model described in Sect. 2.2 and an objective function was calculated using our code in MATLAB [22]. The sample point with the smallest objective function was then used to seed a SCE search.

In order to investigate a range of possibilities for each input parameter and output result, surrogate models are developed to allow for parameter sensitivity analysis and uncertainty quantification [24]. In general, the parameter optimization involves running a series of simulations within the space of input parameters and searching for the best fit of model to experimental data. This SCE approach [27] for high-dimensional and global optimization in PSUADE [17] is coupled with our simulator without modifying the simulation code [25]. The MATLAB [22] version of the simulator is treated as a black box and integrated with the PSUADE [17,26] through input and output variables. One thousand sample points are generated using the Latin hypercube method [23] to cover (i.e., represent) the parametric space and then uncertainties are propagated from model inputs to the output of interest by running the simulator repeatedly on those sample points for sensitivity analyses.

The objective function for our system calibration is defined as

$$\text{Minimization } f = \int_t |m(t) - \hat{m}(t)| dt \tag{11}$$

where $\hat{m}(t)$ [mg] and $m(t)$ [mg] are measured and modeled mass change of the PDMS sample due to diffusion and sorption with

$$m(t) = \rho_\text{b} A_0 \int_0^{x_l} (C_\text{H} + C_\text{L} + C_\text{P})\, dx \tag{12}$$

where ρ_b is the bulk density and A_0 is the sample area. The objective function is minimized using a selected method from PSUADE [17,26] solution library to find the best fit of model to experimental data.

In the case of sensitivity analysis, the approach is similar but the minimization step is omitted. Instead, outputs of simulations (f) on the sample points, are used to construct surrogate models in polynomial formats, and global sensitivity analyses are conducted using the Sobol' method [28] which measures the contribution of each uncertain input to the variance of the output of interest. The total sensitivity index (TSI) of the output is calculated as the sum of all the sensitivity indices including all the interactive effects. Technical details of Sobol' sensitivity approach are given by Saltelli et al. (2008) [29].

3. Results and Discussion

Four physical processes were used to model the experimentally measured moisture uptake in the ideal- and filled-PDMS networks: diffusion, Henry's law absorption, Langmuir adsorption, and pooling. The relative contribution of each process depends on the topology and chemical nature of the material. For example, silica-filler is relatively hydrophilic; hence the filled-PDMS network experiences more Langmuir adsorption than the ideal-PDMS. Eight uncertain parameters (Tables 3 and 4) are considered in the sorption-diffusion model and determined by fitting the model to experimental data. Taking the experimental data as a ground truth, we populate sample points in the parametric space and run the simulations on sample points for evaluating sensitivities of those parameters to the objective function (Eq. (11)). Then, the system parameters are calibrated using the SCE optimization.

3.1. Ideal PDMS

3.1.1. Diffusion-Only Model. To verify the simulation code and demonstrate the calibration process and sensitivity analysis, we performed simulations on the ideal PDMS with the diffusion-only model. When relative humidity is lower than 40%, we believe that both Langmuir adsorption and pooling sorption do not take place in the ideal PDMS, hence,

the simulation depends on only two uncertain parameters: effective diffusivity and effective porosity. In this example, 10,000 sample points are generated on the two-dimensional parametric space, at each temperature, using the Latin hypercube method. Each sample point consists of a value for D and a value for ϕ_e with ranges of $[1.0\times10^{-3} \sim 4.0\times10^{-3}]$ and $[0.010 \sim 0.022]$ respectively. Each sample point is simulated with our mathematical model and the resulting objective function, f, is calculated.

Fig. 3 shows a contour plot of the objective function in the space of D and ϕ_e. In order to better visualize the sensitivity of each parameter, only the 100 best points (i.e., lowest 1% of objective functions) are plotted (red dots) at each temperature. The dashed lines intersect at the sample point with the smallest objective function; this corresponds to the D and ϕ_e values (Table 2) that are optimized for the best fit of experimental data using the SCE method. Fig. 4 shows a comparison of the experimental data with the model using the best-fit parameters. One can see an excellent match of model to experimental results at every temperature.

The contour lines and colors in Fig. 3 indicate a long and narrow valley around each minimum sample point. One can see that the values for effective porosity span a very narrow range at each temperature. This indicates that effective-porosity is a highly sensitive parameter and even a small deviation from the optimal value will produce a poor fit of the model to the data. In contrast, the diffusivity spans a wide range of values at each temperature, which indicates that D is rather insensitive and there is a range of values, all of which will produce a reasonably good fit of the model to the experimental data.

Fig. 5 shows scatter plots of the objective function as a function of each parameter and serves as another method of visualizing the data in Fig. 3. One can clearly see that there is a wide range of effective diffusivity values that result in similar objective functions and therefore the diffusivity is an insensitive parameter. In contrast, the effective porosity comes to a sharp point at each temperature and even a small deviation away from the minimum results in a significant change in the objective function.

The Sobol' sensitivity approach is a quantitative method of assessing parameter sensitivity. The Sobol' total sensitivity indices (TSI) provide a ranking for relative sensitivity of parameters. The most sensitivity parameter gets the largest TSI value and less sensitive parameters have smaller TSI values commensurate with their relative sensitivity. The TSI values for this example are listed in parentheses in Table 2 and are consistent with the conclusions reached in Figs. 3 and 5.

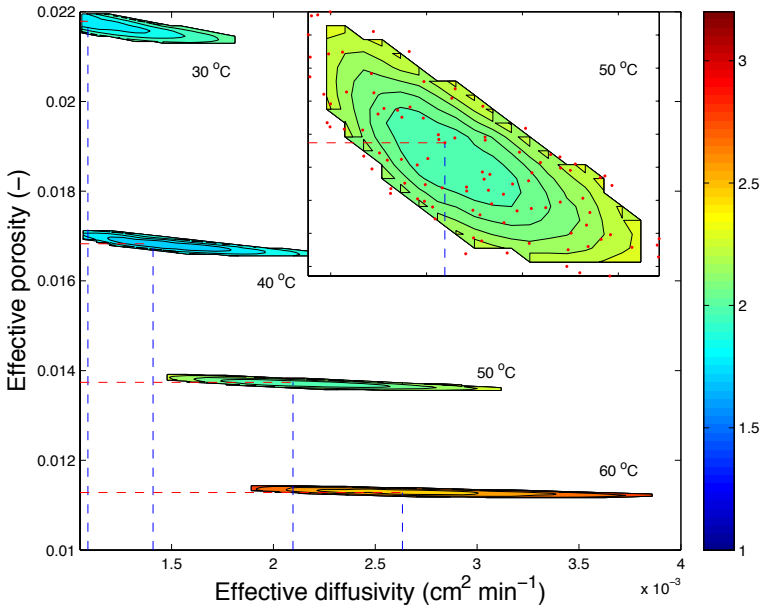

Figure 3. Response surface of objective function, f, in term of diffusivity and effective porosity. The upper-right plot is the zoomed-in valley area of objective function at 50 °C. Red dots represent the sample points, only the sample points with the smallest objective functions are plotted (lowest 1%). Dashed lines indicate locations of minima.

Table 2. Optimized diffusivity and effective porosity at various temperatures in ideal PDMS.

Parameter	Symbol	Calibrated results			
		30 °C	40 °C	50 °C	60 °C
Effective diffusivity	$D\times10^3$	1.0891 (0.0020)[1]	1.4086 (0.0143)	2.0957 (0.0093)	2.6331 (0.0052)
Effective porosity	$\phi_e\times10^2$	2.1789 (1.0000)	1.6829 (1.0000)	1.3737 (1.0000)	1.1283 (1.0000)
Objective function	f	1.7716	1.6947	1.9722	2.4523

[1]Numbers in parentheses indicate Sobol' total sensitivity.

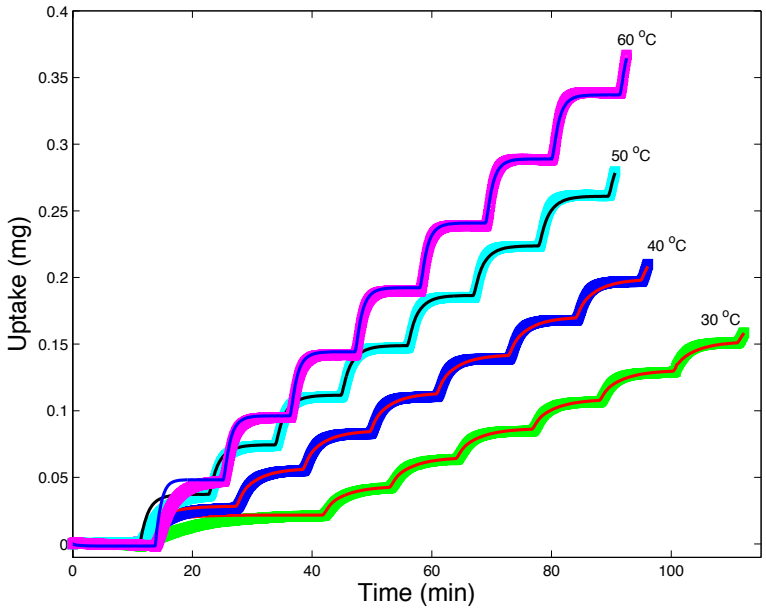

Figure 4. Comparison of moisture-mass uptake between calibrated-model results (solids lines) and experimental data (circles) in ideal PDMS at 30, 40, 50, and 60 °C.

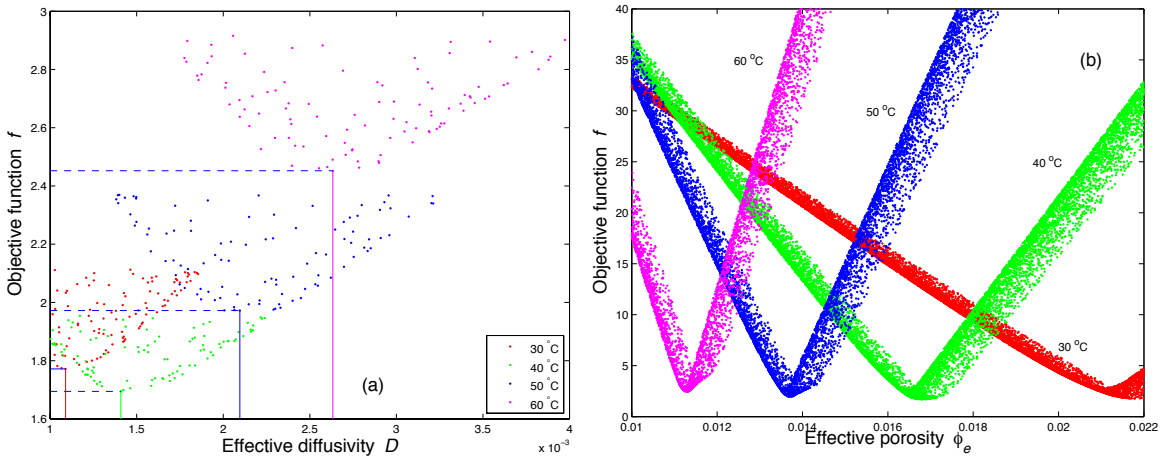

Figure 5. Scatter plots of objective function as a function of (a) diffusivity and (b) effective porosity at four temperatures (30, 40, 50 and 60 °C). Note that only 100 best sample points are plotted in (a) to view the global minima.

3.1.2. Triple-mode Sorption. In order to fit the ideal-PDMS data from 0 to 95% RH, our triple-mode sorption model was necessary (Eqs. (8) and (9)). All attempts to fit the ideal-PDMS over this range with a diffusion-only model resulted in poor fits. Figs. 6a and 6c show comparisons of the experimentally measured moisture-mass uptake with the triple-mode optimized-model and the diffusion-only optimized-model at 30, 40, 50, and 60 °C. The relative error for each of these models is also plotted in Figs. 6b and 6d. One can see that the triple-mode sorption model (solid lines) overlaps quite well with the experimental data (dots) at every RH step and every temperature; only the first RH-step (i.e., 15 to 40 min) at all four temperatures shows an imperfect match (with up to 2.6% error) between model and experiment (Fig. 6b). This mismatch is likely due to the concentration-dependent diffusivity at low relative humidities, which is not considered in this study. In the diffusion-only model

(Fig. 6c), the match between experiment and model is reasonably good up to about 75% RH (i.e., 180 min) at which point the model can no longer match the experimental data. A plot of relative error (Fig. 6d) illustrates the poor match between experiment and model when a diffusion-only model is used at a high RH ($> 75\%$).

A plot of the relative contribution of each mode (see, for example, Fig. 8) reveals that Langmuir adsorption makes a negligible contribution to the total mass uptake. Thus, the mechanisms of moisture uptake in the ideal-PDMS are Henry's law absorption and pooling. Logically this makes sense, the ideal-PDMS is expected to be hydrophobic and contain no hydrophilic filler materials; therefore nothing in the material can adsorb moisture via the Langmuir mechanism.

Fig. 7 shows the model results for total uptake (upper bound of each filled curve) and Henry's absorption (lower bound of each filled curve) at each temperature. The shaded region between these two curves is the uptake from pooling. One can see that the Henry's law absorption is responsible for most of the moisture that is sorbed into the material. Pooling of water molecules began at about 50% RH (i.e., >120 min).

Table 3 lists the optimized values for the eight uncertain parameters of the ideal-PDMS model at 30, 40, 50, and 60 °C (note that k_{ads} was not considered as an independent parameter in the optimization process, rather it is calculated here based on the parameters k_{des} and b'). One can see that the optimized Langmuir parameters (i.e., C'_{H}, b' and k_{ads}) are all small values. The pooling threshold value (i.e., C^0_{H}) was optimized at 0.35367, 0.53661, 0.63559, and 0.74380 [mg g^{-1}], for four temperatures; essentially this parameter indicates that pooling initiates when the Henry's concentration (i.e., C_{H}) exceeds the threshold values. These parameters will be discussed in more detail in Sect. 3.2, in comparison with the filled-PDMS parameters.

With the calibrated pooling parameters, the pooling concentration in the ideal PDMS is calculated using Eq. (10) with the calibrated α, C^0_{H}, and n in Table 3. The power-law relation depends on the difference between Henry's concentration and the threshold value rather than on Henry's concentration directly.

Table 3. Optimized parameters at various temperatures in the ideal PDMS.

Parameter	Symbol	Calibrated results			
		30 °C	40 °C	50 °C	60 °C
Effective diffusivity	D	1.5105×10^{-3}	1.8509×10^{-3}	2.5556×10^{-3}	3.6061×10^{-3}
Desorption rate	k_{des}	6.0367×10^{-4}	1.0716×10^{-4}	7.5837×10^{-5}	7.7426×10^{-5}
Langmuir capacity	C'_{H}	5.7306×10^{-3}	8.8910×10^{-3}	1.8440×10^{-2}	1.4551×10^{-3}
Langmuir affinity	b'	1.0093×10^{-1}	8.9940×10^{-1}	8.6285×10^{-1}	7.7043×10^{-2}
Pooling factor	α	4.6835×10^{-1}	4.2784×10^{-1}	5.1201×10^{-1}	1.4848×10^{-1}
Pooling threshold	C^0_{H}	3.5367×10^{-1}	5.3661×10^{-1}	6.3559×10^{-1}	7.4380×10^{-1}
Pooling power	n	1.4128	1.3875	2.1391	1.0881
Effective porosity	ϕ_e	2.1947×10^{-2}	1.7011×10^{-2}	1.3743×10^{-2}	1.1283×10^{-2}
Adsorption rate	$k_{\text{ads}} = b'k_{\text{des}}$	6.0925×10^{-4}	9.6380×10^{-5}	6.5436×10^{-5}	5.9948×10^{-6}
Objective function	f	2.0791	2.3719	3.3023	3.7254

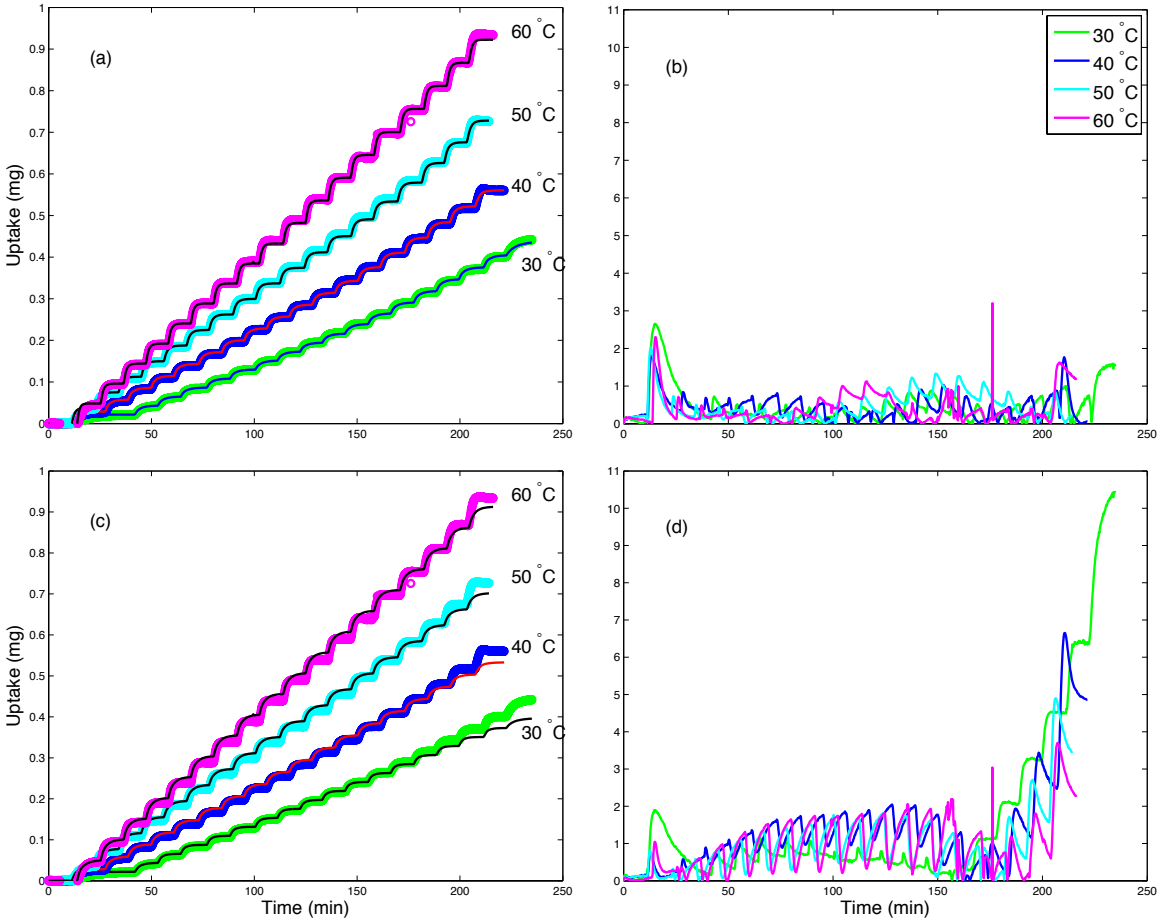

Figure 6. Comparison of moisture-mass uptake between calibrated-model results and experimental data in ideal PDMS at 30, 40, 50, and 60 °C. (a) Comparison between modeled and measured uptakes using the triple-mode sorption model (Eqs. (8) and (9)). (b) Relative error using the triple-mode sorption model. (c) Comparison between modeled and measured uptake using the diffusion-only model. (d) Relative error using the diffusion-only model. Each uptake step results from a step up in relative humidity in the chamber, refer to Fig. 1 for a plot of RH and mass-moisture uptake.

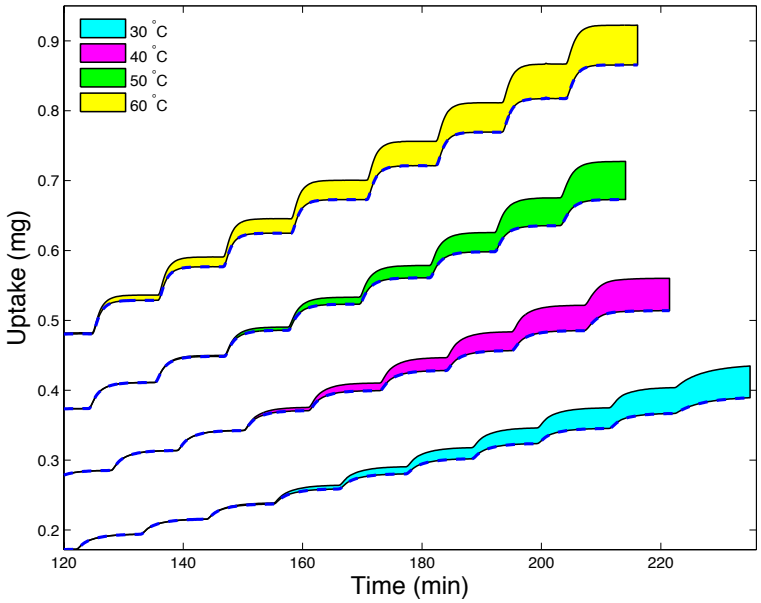

Figure 7. Comparison of the ideal-PDMS total uptake (upper bound of each filled curve) and Henry's absorption (lower bound of each filled curve) at each temperature. The filled area corresponds to the contribution from pooling; note that pooling sorption starts at high relative humidity.

Fig. 8 shows the concentrations (Henry's, Langmuir, pooling, and total) as functions of time at the center of the ideal PDMS sample at 30, 40, 50, and 60 °C. Although the total concentration at the boundary corresponds well with that of the environmental relative humidity (Figs. 1a, b), the total concentration at the center (i.e., depth = 0.1 cm), as shown in Fig. 8 shows the time lag due to the diffusion from the boundary to the center. These plots highlight the subtle details that can be extrapolated from the experimental data with the aid of our high fidelity modeling approach.

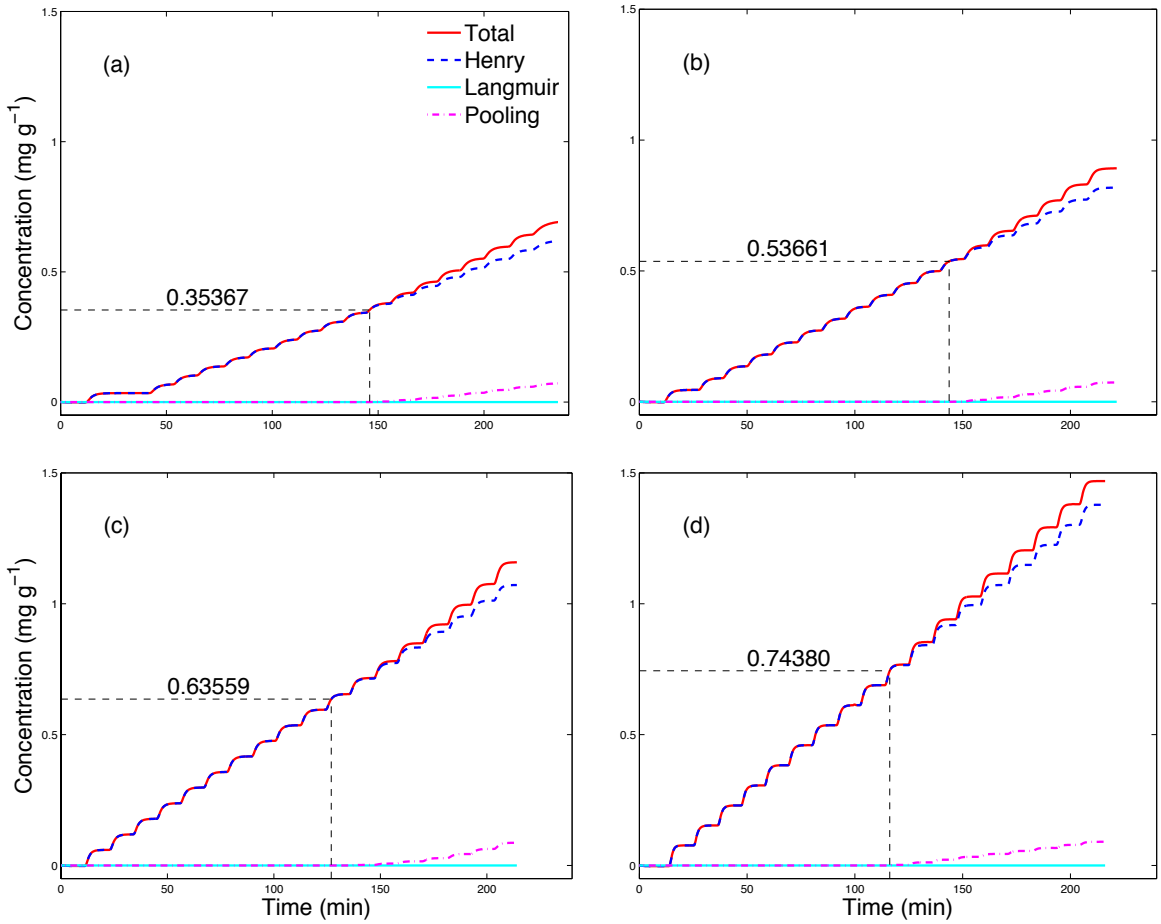

Figure 8. Concentrations as functions of time at the center of the ideal PDMS sample at (a) 30, (b) 40, (c) 50, and (d) 60 °C.

3.2. Filled PDMS

Fig. 9 shows a comparison of the experimental and modeled moisture-mass uptake of the filled-PDMS using the triple-mode model between 0 and 95% RH. One can see an excellent match between the total model (black line) and experimental data (red circles). Each of the three sorption modes (Henry, Langmuir, and pooling) is plotted independently in the figure. The Langmuir contribution appears to be the dominant sorption mechanism, especially at lower humidities; in sharp contrast with the ideal-PDMS network where Langmuir adsorption was insignificant. Henry's law absorption in the sample makes a relatively small contribution to the total mass uptake. Pooling mechanisms become active at 75% relative humidity. Attempts to fit the filled PDMS results to a diffusion-only model (with effective diffusivity and effective porosity only) resulted in extremely poor match of model to experiment necessitating the triple-mode model.

It is observed that the experimental curve changes shape above the 75% RH step. This experiment was duplicated and the same response at 75% RH was measured repeatedly. One can see in Fig. 9 that above 75% RH the rise time at each RH step is significantly slower than the previous RH steps; this suggests that diffusivity is different at these higher RHs. Also, above 75% RH, the amount of moisture that is taken up in each RH step is substantially larger than the moisture uptake in the lower RH steps; this suggests that the pooling mechanism may reduce the tortuosity in the porous medium. It is interesting to note that 75% RH is also the point where the Langmuir adsorption reaches its capacity,

which suggests that the change in behavior of the material may be due to the Langmuir-site saturation. In order to achieve the excellent match of model to experiment that is demonstrated in Fig. 9, a reduced tortuosity was introduced at the point when pooling started (i.e., above 75% RH), below this point the tortuosity was 1.0. The effective diffusivity reported in Table 4 is the value before pooling initiates (i.e., tortuosity = 1, therefore $D = D_0$). Once pooling begins, the effective diffusivity can be calculated based on $D = D_0\,\tau$ (i.e., effective diffusivity = $8.5003\times10^{-5} = 1.6452\times10^{-3}\times5.1667\times10^{-2}$). Thus, the reduced tortuosity permits the effective diffusivity to decrease in order to match the slow rise-times observed above 75/in Fig. 9. As stated above, the filled-PDMS is most likely experiencing some change (e.g., swelling and/or plasticization) that results in a change in the mechanisms of pooling and diffusion.

Table 4 (column 5) lists the optimized parameters for the filled-PDMS triple-mode model. One can see a striking difference between the filled and ideal-PDMS parameters for Langmuir capacity, Langmuir affinity, and desorption rate. The Langmuir capacity of the filled PDMS is about 400∼5000 times larger than the ideal-PDMS. These numbers are consistent with the fact that the silica-filler in the filled-PDMS is hydrophilic [9,20,21]. The larger desorption rate in the filled PDMS is complimented by a large Langmuir affinity (b'). Keeping in mind that $b' = k_{\text{ads}}/k_{\text{des}}$, one can calculate k_{ads} for the ideal-PDMS (e.g., 9.6380×10^{-5} at 40 °C) and filled-PDMS (1.4240×10^{-1}) and see that the filled-PDMS adsorbs and desorbs moisture at a high rate compared with the ideal-PDMS. In other words, moisture in the filled-PDMS is constantly being attracted and van der Waals bonded to the silica filler although the desorption rate is high, the adsorption rate is even higher resulting in a large population of water molecules that are adsorbed into the material. The diffusivity is nearly the same in the filled and ideal-PDMS materials, this makes sense since both materials consist of a similar hydrophobic polymeric network.

Finally, the pooling parameters in ideal- and filled-PDMS are different from each other, which is not surprising considering the different chemical and mechanical properties of the materials. In addition, the Sobol' sensitivity analysis of the objective function (Eq. 11) in terms of all parameters on the filled PDMS network showed that the effective porosity (ϕ_e) and the pooling threshold (C_{H}^0) are the most important of all the parameters. Hence, the differences in pooling parameters between the ideal- and filled-PDMS are expected to have very little impact on the overall model outcome. With the calibrated pooling parameters in Table 4 (column 5), the pooling concentration in the filled PDMS is specified using Eq. (10).

Table 4. Filled-PDMS parameters: input ranges, calibrated values, and Sobol' sensitivities of experiment 5.

Parameter	Symbol	Min	Max	Optimized	Sobol' TSI	TSI rank
Effective diffusivity	D	1.0×10^{-4}	3.2×10^{-3}	1.6452×10^{-3}	1.7160×10^{-4}	8
Desorption rate	k_{des}	1.0×10^{-2}	1.0×10^{-1}	5.4505×10^{-2}	4.9072×10^{-5}	9
Langmuir capacity	C'_{H}	5.0	9.0	7.3054	2.6169×10^{-2}	3
Langmuir affinity	b'	1.0	1.0×10^{1}	2.6126	9.7824×10^{-3}	4
Pooling factor	α	1.0×10^{1}	1.5×10^{1}	1.2583×10^{1}	4.7434×10^{-3}	5
Pooling threshold	C_{H}^0	1.24	3.0	1.8580	5.1070×10^{-1}	2
Pooling power	n	1.0	1.24	1.0180	2.3161×10^{-3}	7
Effective porosity	ϕ_e	5.0×10^{-2}	1.0×10^{-1}	6.1812×10^{-2}	5.1852×10^{-1}	1
Reduced tortuosity	τ	2.7×10^{-2}	8.5×10^{-1}	5.1667×10^{-2}	2.4485×10^{-3}	6
Adsorption rate	$k_{\text{ads}} = b'k_{\text{des}}$	-	-	1.4240×10^{-1}	-	-

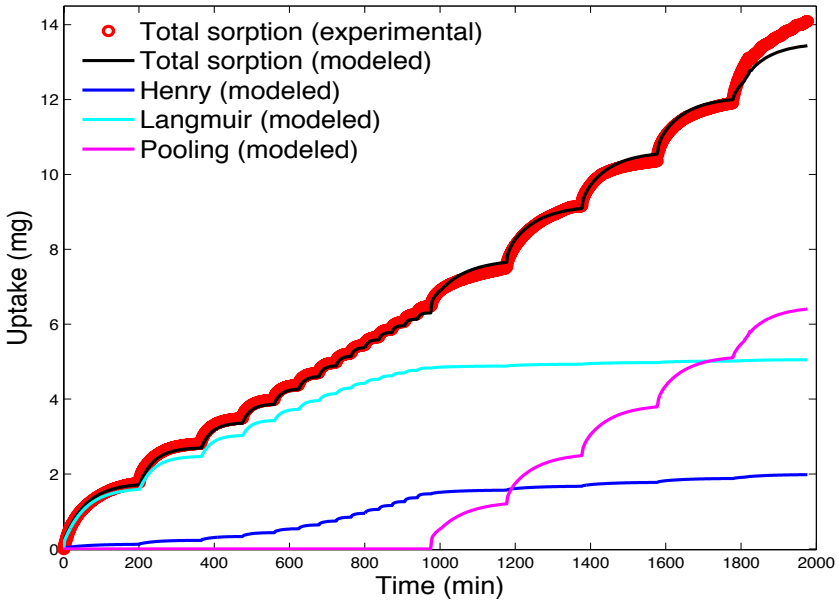

Figure 9. Comparison of moisture-mass uptake between calibrated model results and experimental data in the filled-PDMS. Each uptake step results from a step up in relative humidity of the chamber, refer to Fig. 1b for a plot of RH and mass/moisture uptake.

Fig. 10 shows the Henry, Langmuir and pooling concentrations as functions of time at the boundary and the center of filled PDMS. One can see how fast the boundary concentration plot (Fig. 10a) responds to the change of the chamber-environment RH (Fig. 1b). In contrast, the concentration curves at the center (Fig. 10b) show the time lag due to the diffusion from the boundary to the center. These plots highlight the subtle details that can be extrapolated from the experimental data with the aid of our high fidelity modeling approach.

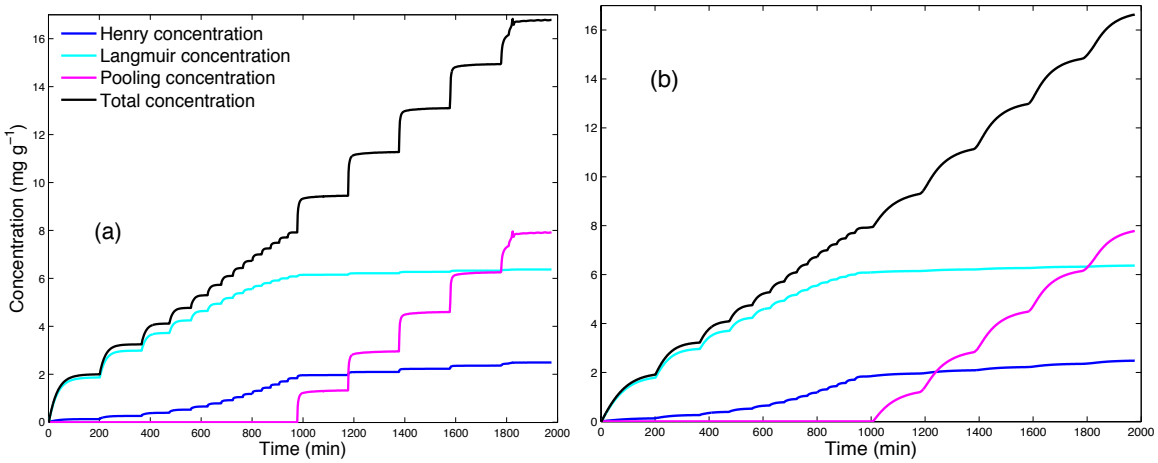

Figure 10. Concentration as a function of time at (a) boundary and (b) center of filled PDMS.

3.3. Uncertainty Quantification of *Decision Variables*

Uncertainty quantification is an important, although often omitted, step in predictive modeling. In Sections 3.1 and 3.2 the calibration parameters were optimized and a Sobol' sensitivity analysis was performed on them. Throughout that analysis, we assumed that

the RH and sample thickness were well defined and free of uncertainty. In reality, both RH and thickness are variables that will affect the outcome of the mass-uptake calculations and their uncertainties must be accounted for. We have termed these variables *decision-variables* and here we investigate the impact of uncertainties of these decision-variables on the mass uptake.

For a given relative humidity and a PDMS thickness, mass uptake asymptotically converges to an equilibrium level due to vapor diffusion and triple-mode sorption. To quantify the equilibrium uptake as a function of relative humidity and thickness, we measure the ratio of the uptake [mg] to the initial mass of dry PDMS [g]:

$$\lambda = \frac{\int_0^{x_l} (C_{\mathrm{H}} + C_{\mathrm{L}} + C_{\mathrm{P}})\, dx}{x_l} \tag{13}$$

where x_l [cm] is the PDMS thickness. λ is a measure of concentration and reflects the sorbed mass in milligram per gram of dry PDMS. The *equilibrium time* required to reach equilibrium is measured as t_λ when $d\lambda/dt \leq 1.0\times10^{-4}$, which is estimated to be the point where the system has reached equilibrium.

We explored the impact of these two decision variables by creating an array of 1000 sample points in the space of RH and thickness (i.e., 1000 different combinations of RH and thickness). The model was run 1000 times using optimized parameters of the ideal-PDMS at 40 °C (Column 4 of Table 2). The procedure was repeated with the filled-PDMS optimized parameters listed in Table 4 and an array of 1000 sample points appropriate for the filled-PDMS system. The results are discussed below.

3.3.1. Equilibrium Uptake of Ideal PDMS. The dependence of the mass ratio, λ, and equilibrium time, t_λ, on PDMS thickness and relative humidity are plotted in Fig. 11. One can see in Fig. 11a that there is a range of mass ratios that will result when the thickness is varied, with no evident trend. This plot demonstrates that the mass ratio is not influenced by the thickness; this is as it should be, the material is truly reaching equilibrium. Fig. 11b shows a strong dependence of mass ratio on relative humidity; this conclusion is logical since one would expect the sample to sorb more water when the relative humidity is higher. The linear relation between the equilibrium uptake ratio and relative humidity for RH$\leq$ 60% in Fig. 11b reflects the Henry's absorption. The slight nonlinear behavior for RH$>$ 60% is due to the pooling sorption. Figs. 11c and 11d indicate that the equilibrium time is mainly controlled by the thickness with no strong influence by the relative humidity. Again, these results are logical, since a thicker sample will take longer to reach equilibrium due to diffusion. A Sobol' global sensitivity analysis of the results quantifies the contributions of relative humidity and thickness to both λ and t_λ (see Table 5). In addition to the plots, which qualitatively show the dependencies, the Sobol' analysis provides a quantitative measure for interpreting the results.

Table 5. Sobol' sensitivity indices of relative humidity and PDMS thickness to equilibrium uptakes.

PDMS	Output	PDMS thickness (cm)		Relative humidity	
		First-order	Total sensitivity index	First-order	Total sensitivity index
Ideal	λ	1.0019×10^{-7}	1.7730×10^{-6}	9.9387×10^{-1}	1.1013
	t_λ	8.6891×10^{-2}	9.8944×10^{-1}	8.7546×10^{-3}	9.0231×10^{-3}
Filled	λ	1.5276×10^{-4}	7.2003×10^{-4}	1.0000	1.0981
	t_λ	9.9621×10^{-2}	7.1617×10^{-1}	2.7599×10^{-1}	1.2668

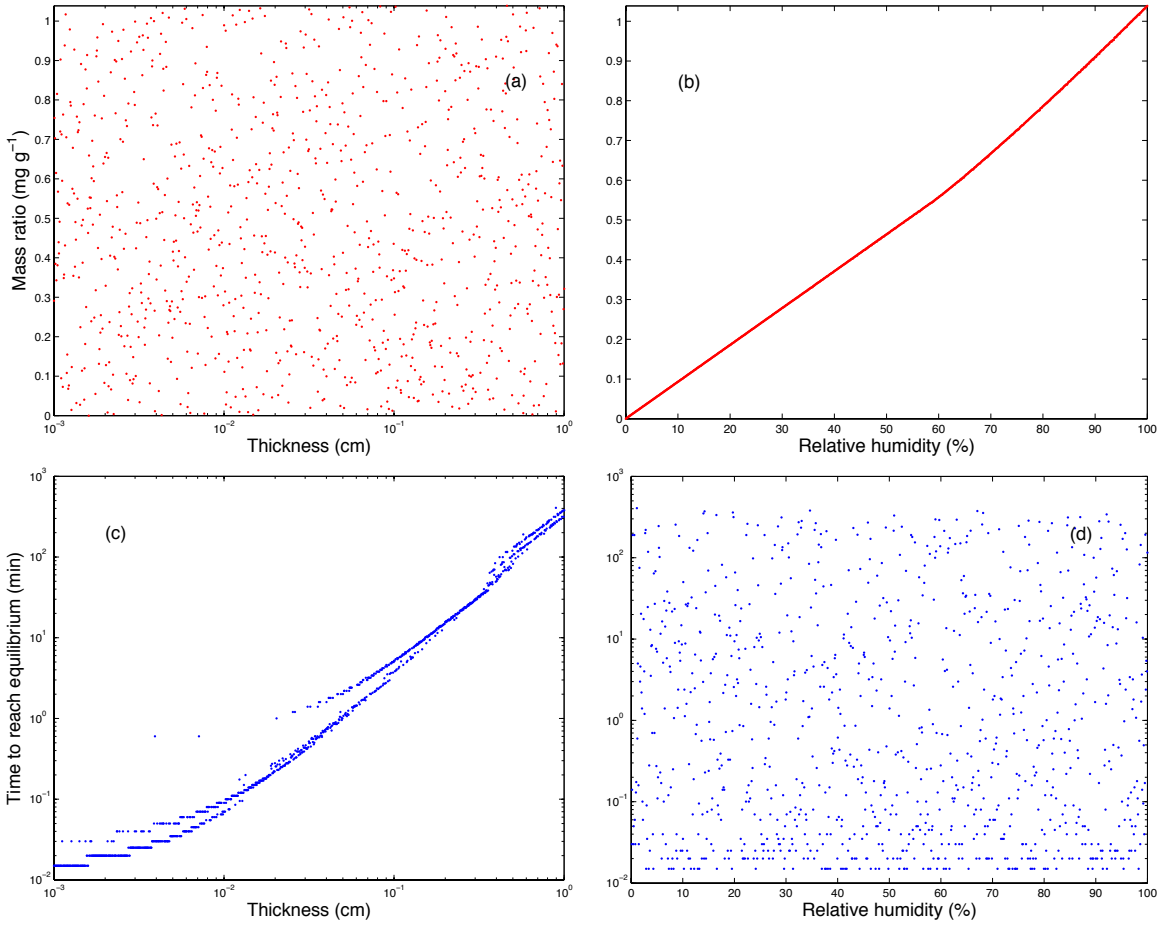

Figure 11. Scatter plots of the dependence of the equilibrium uptake and the time to reach the equilibrium in ideal PDMS. (a) Mass ratio, λ, as a function of PDMS thickness. (b) Mass ratio, λ, as a function of relative humidity. (c) Equilibrium time, t_λ, as a function of PDMS thickness. (d) Equilibrium time, t_λ, as a function of relative humidity.

3.3.2. Equilibrium Uptake of Filled-PDMS. Fig. 12 shows the dependence of the equilibrium uptake mass ratio, λ, and equilibrium time, t_λ, on sample thickness and relative humidity in the filled PDMS. Comparison of Figs. 12a and 12b reveal no dependence of mass ratio, λ, on sample thickness but a strong dependence on relative humidity. Fig. 12b also demonstrates the nonlinear process due to the dominant Langmuir adsorption in the filled PDMS and a dramatic change in the curve in Fig. 12b which corresponds to the point when pooling begins (see Fig. 13b).

Figs. 12c and 12d indicate that both thickness and RH influence the equilibrium time. Fig. 12c indicates that when the sample gets very thick there is a minimum equilibration time, presumably due to diffusion, which will be retarded by the Langmuir and pooling sorption processes. Fig. 12d shows that at the lower relative humidities there is a minimum time to reach equilibrium. The sorption process in the filled-PDMS at these humidities is dominated by Langmuir adsorption, which is not instantaneous since (1) a water molecule must locate a Langmuir sorption site and (2) a van der Waals bond must be formed. Hence at low RH, there is some minimum time required to reach equilibrium as the small population of water molecules locate Langmuir sorption sites. As the RH increases, the probability of a water molecule to locate a Langmuir site increases and the time to reach equilibrium drops. Sobol' global sensitivity analysis (Table 5) quantifies the relative importance of thickness and RH to the mass ratio and equilibrium time for the filled-PDMS.

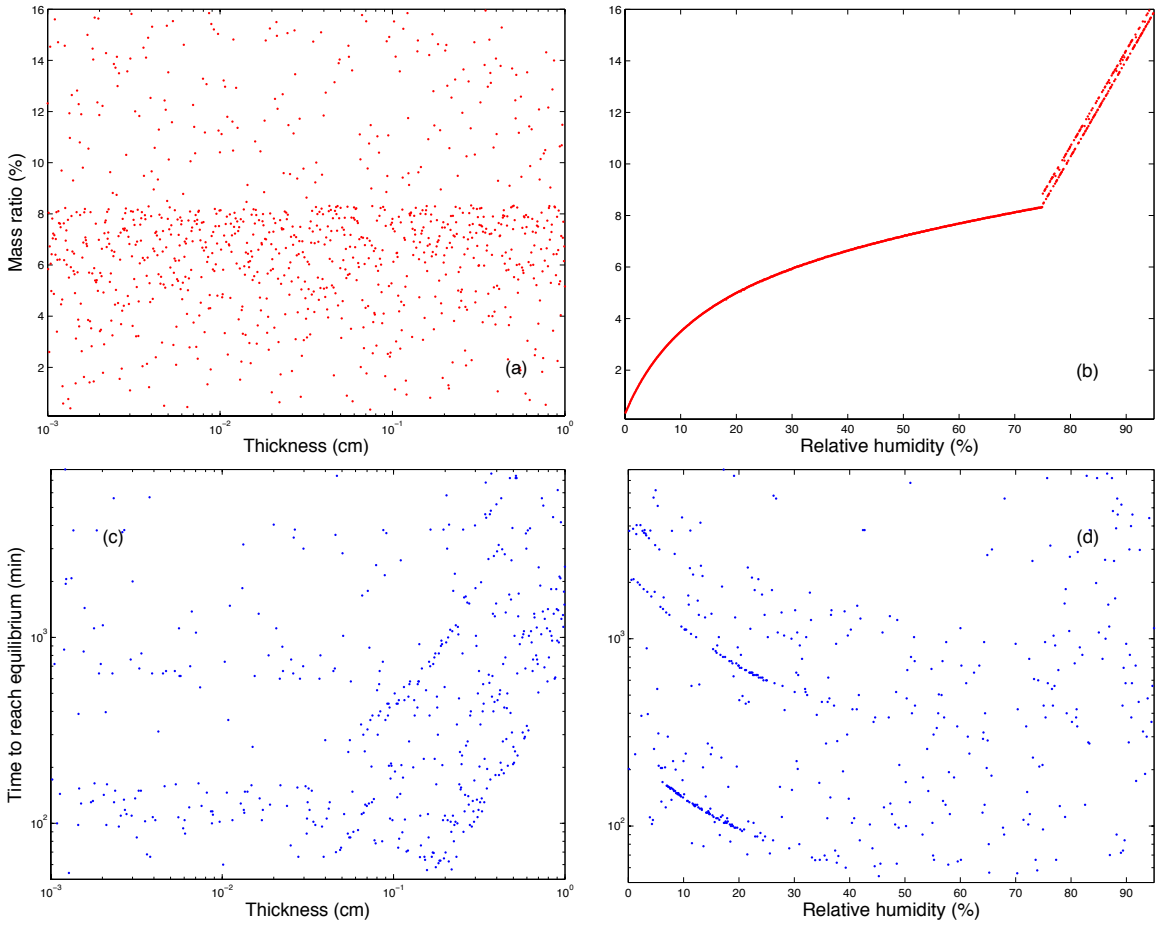

Figure 12. Scatter plots of the dependence of the equilibrium uptake and the time to reach the equilibrium in filled-PDMS. (a) Mass ratio, λ, as a function of PDMS thickness. (b) Mass ratio, λ, as a function of relative humidity. (c) Equilibrium time, t_λ, as a function of PDMS thickness. (d) Equilibrium time, t_λ, as a function of relative humidity.

In order to determine how RH and sample thickness influence the mass-ratio of each sorption mechanism, the partial ratio of equilibrium uptake for each sorption mode was defined

$$\lambda_i = \frac{\int_0^{x_l} C_i dx}{x_l}, \quad i = \text{H, L, P} \tag{14}$$

and measured as functions of relative humidity and PDMS thickness as shown in Fig. 13. In Fig. 13a one can see that the distribution of mass-ratio values range from 0 to approximately 2.5 [g mg^{-1}] for the Henry absorption but span the full range from 0 to 6.5 [g mg^{-1}] for the Langmuir and pooling mechanisms. This trend is expected as there is only a small population of water that resides in the material via Henry's absorption. Other than the maximum sorption capacity for each mechanism, there is no trend between thickness and mass-ratio of sorbed water. In contrast, there is a strong trend in the mass-ratio and the RH, as is shown in Fig. 13b.

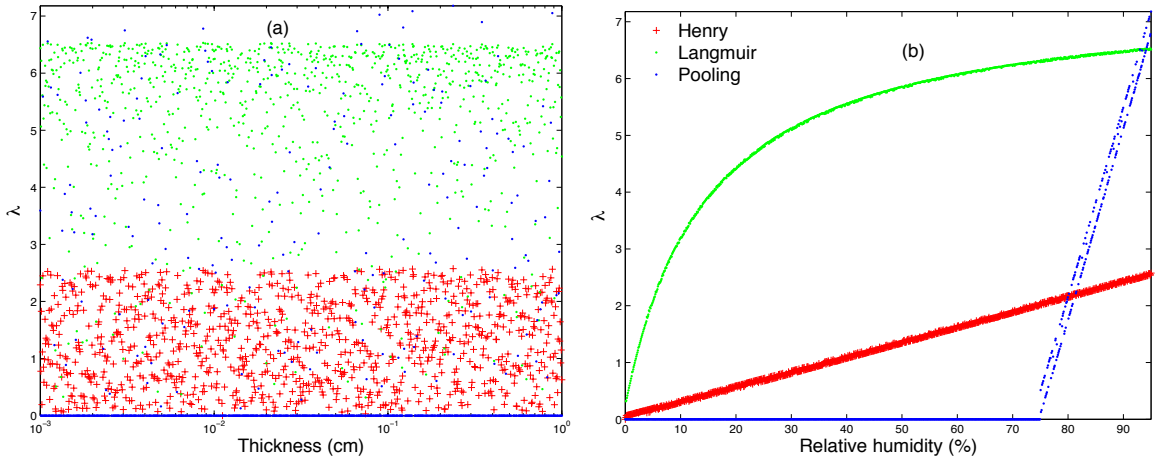

Figure 13. Partial ratios of equilibrium uptake as functions of (a) PDMS thickness and (b) relative humidity.

4. Conclusions

Modeling of the vapor sorption and diffusion in a material is a challenging problem with a range of applications. Most models are limited to a narrow range of humidities and are unable to model dynamic sorption and diffusion processes. The improvements in experimental methods for measuring vapor-uptake have made it possible and necessary to extend our modeling capabilities. A model that can capture both dynamic and equilibrium sorption of a vapor is quite useful for characterizing and understanding the nature of the material and extremely useful for predicting the uptake and/or outgassing quantities and rates in non-equilibrium conditions.

The model presented here was exercised and verified with a simple, established, and well characterized material and vapor: poly(dimethylsiloxane) (PDMS) and water, respectively. Two different PDMS materials were investigated, a silica filled-PDMS and an ideal-PDMS (i.e., unfilled). Vapor diffusion coupled with Henry's law absorption, Langmuir adsorption, and pooling sorption in ideal and filled-PDMS materials were systematically calibrated using experimental data and SCE global optimization. Triple-mode sorption processes, including kinetic Langmuir adsorption, equilibrium Henry's law absorption and pooling sorption, were modeled, coupled with diffusion equation, and solved using an operator-splitting scheme. The deterministic but physics-based simulation is further coupled with PSUADE, an uncertainty quantification tool, for calibrating uncertain system processes and parameters. Using this solution scheme together with experimental data, we highlight the following insights:

1. Kinetic Langmuir adsorption, equilibrium Henry's absorption, and pooling sorption can be distinguished and formulated at the continuum scale.

2. Effective diffusivity can be treated as a product of molecular-weight-dependent binary diffusivity and material-specific tortuosity and calibrated using the total uptake measurement. The calibrated effective diffusivity in the ideal and filled PDMS is close to the value derived by Watson and Baron (1996) [30].

3. As a power-law function of Henry's concentration, pooling concentration depends on a threshold value of Henry's concentration. When Henry's concentration exceeds the threshold value, pooling occurs and its concentration is a power-law function of the difference between Henry's concentration and the threshold.

4. In addition to diffusion, Henry's absorption is the dominant physical process for the total uptake in the ideal PDMS, while Langmuir adsorption is the major contributor to the uptake in filled PDMS when boundary relative humidity is below 75.36%.

5. In the filled PDMS, pooling initiates and becomes the dominant sorption process after Langmuir concentration asymptotically converges to its equilibrium (RH $>$ 75.36%). The effective diffusivity is significantly reduced at this critical point.

The model developed here was designed to succeed with a variety of membranes or materials and vapors and work is underway to characterize other materials of interest to the scientific and engineering communities. Our results demonstrate how the model can be used and the parameters that can be extracted from the experimental results. Our sensitivity analysis and uncertainty quantification are particularly unique and empower us to explore a range of outcomes without laborious experiments or changes to the model. With this mathematical model and parameters, one can predict the uptake or outgassing of a material or an assembly of materials in a realistic geometry. Thus, predicting a realistic timeframe for a vapor to outgas from or sorb into a material can be achieved with simple experiments and this sophisticated model. Applications range from predicting vapor intrusion rates through protective or separation membranes to predicting vapor desorption and outgassing from a membrane that has experienced a change in environmental conditions.

Acknowledgements

This work was conducted under the auspices of the U.S. Department of Energy by Lawrence Livermore National Laboratory under contract DE-AC52-07NA27344.

References

[1] V. Detallante, D. Langevin, C. Chappey, R. Métayer, M. Mericier, M., Pinéri, Water vapor sorption in naphtalenic sulfoanted polyimide membranes, J. Membr. Sci. 190 (2001) 227–241.

[2] V. Detallante, D. Langevin, C. Chappey, R. Métayer, M. Mericier, M. Pinéri, Kinetics of water vapor sorption in sulfonated polyimide membranes, Desalination 148 (2002) 333–339.

[3] G.S. Park, J. Crank, *Diffusion in polymers* Academic Press Publisher, New York, pp. 452, 1968.

[4] J. Crank, *The Mathematics of Diffusion*, Oxford University Press, Oxford, NY, pp. 414, 1979.

[5] V. Stannet, The transport of gases in synthetic polymeric membranes, an historic perspective, J. Membr. Sci. 3(2) (1978) 97–115.

[6] W.J. Koros, D.R. Paul, CO_2 sorption in poly(ethylene terephthalate) above and below the glass transition, J. Polym. Sci. 16(11) (1978) 1947–1963.

[7] W.R. Vieth, J.M. Howell, J.H. Hsieh, Dual sorption theory, J. Membr. Sci. 1 (1976) 177–220.

[8] S.J. Harley, E.A. Glascoe, R.S. Maxwell, Thermodynamic study on dynamic water vapor sorption in sylagrd-184, J. Phys. Chem. 116 (2012) 14183–14190.

[9] S.J. Harley, E.A. Glascoe, J.P. Lewicki, R.S. Maxwell, Advances in modeling sorption and diffusion of moisture in porous reactive materials, Chem. Phys. Chem. 15(9) (2014) 1809–1820.

[10] E. Favre, P. Schaetzel, Q.T. Nguygen, R. Clément, J. Néel, J., Sorption, diffusion and vapor permeation of various penetrants through dense poly(dimethylsiloxane) membranes: a transport analysis, J. Membr. Sci. 92(2) (1994) 169–184.

[11] T.C. Merkel, V.I. Bondar, K. Nagai, B.D. Freeman, I. Pinnau, Gas sorption, diffusion, and permeation in poly(dimethylsiloxane), J. Polymer Sci. Part B: Polymer Physics 38(3) (2000) 415–434.

[12] S.C. George, S. Thomas, Transport phenomena through polymeric systems, Prog. Polym. Sci. 26(6) (2001) 985–1017.

[13] Tsujita, Gas sorption and permeation of glassy polymers with microvoids, Prog. Polym. Sci. 28 (2003) 1377–1401.

[14] F. Wu, L. Li, Z. Xu, S. Tan, Z. Zhang, Transport study of pure and mixed gases through PDMS membrane, Chem. Eng. J. 117(1) (2006) 51–59.
[15] J. Guo, T.A. Barbari, A dual mode, local equilibrium relaxation model for small molecule diffusion in a glassy polymer, Macromolecules 41(1) (2008) 238–245.
[16] C. Lu, Y. Sun, S.J. Harley, E.A. Glascoe, Modeling gas transport and reactions in polydimethylsiloxane Proceedings of TOUGH Symposium 2012, Lawrence Berkeley National Laboratory, Berkeley, California, September 17–19 (2012).
[17] C. Tong, *PSUADE User's Manual*, Lawrence Livermore National Laboratory, LLNL-SM-407882, 2005.
[18] B. Boonstra, Role of particulate fillers in elastomer reinforcement: a review, Polymer 20(6) (1979) 691–704.
[19] C.C. Sun, J.E. Mark, Comparisons among the reinforcing effects provided by various silica-based fillers in a siloxane elastomer, Polymer 30(1) (1989) 104–106.
[20] R.S. Maxwell, L. Dinh, R. Gee, B. Balazs, Experimental and modeling studies of water-silica-PDMS interactions in M97-based stress cushions, Lawrence Livemore National Laboratory, UCRL-JC-148029 (2002).
[21] L.N. Dinh, A.K. Burnham, M.A. Schildbach, R.A. Smith, R.S. Maxwell, B. Balazs, W. McLean II, Measurement and prediciton of H_2O outgassing kinetics from silica-filled polydimethylsiloxane TR55 and S5370, J. Vac. Sci. Technol. A 25(3) (2007) 597–600.
[22] MathWorks, *MATLAB high-performance numeric computation and visualization software*. Web site: www.mathwroks.com, Natick, MA, USA, 2000.
[23] M.D. McKay, R.J. Beckman, W.J. Conover, A comparison of three methods for selecting values of input variables in the analysis of output from a computer code, Technometrics 21(2) (1979) 239–245, doi:10.2307/1268522.
[24] Y. Sun, C. Tong, Q. Duan, T.A. Buscheck, J.A. Blink, J.A., Combining simulation and emulation for calibrating sequentially reactive transport systems, Transp. Porous Med. 92(2) (2012) 509–526.
[25] Y. Sun, J.N. Petersen, J. Bear, Successive identification of biodegradation rates for multiple sequentially reactive contaminants in groundwater J. Contam. Hydrol. 51(1–2) (2001) 83–95.
[26] C. Tong, Self-validated variance-based methods for sensitivity analysis of model outputs, Reliab. Eng. Syst. Safe. 95(3) (2010) 301–309.
[27] Q. Duan, S. Sorooshian, V. Gupta, Effective and efficient global optimization for conceptual rainfall-runoff models, Water Resour. Res. 28(4) (1992) 1015–1031.
[28] I. Sobol', Sensitivity analysis for nonlinear mathematical models, *Mathematical Modeling & Computational Experiment* 1 (1993) 407–414, (English translation from Russian original paper Sobol', 1990).
[29] A. Saltelli, M. Ratto, T. Andres, F. Campolongo, J. Cariboni, D. Gatelli, M. Saisana, S. Tarantola, Global Sensitivity Analysis, The Primer, John Wiley & Sons (2008), pp. 292.
[30] J.M. Watson, M.G. Baron, The behaviour of water in poly(dimethylsiloxane), J. Membr. Sci. 110(1) (1996) 47–57.

This preprint was prepared with Yunwei Sun's LaTeX macros v4. File sorption8 formatted November 3, 2014.